Electronic Journal of Biotechnology 70 (2024) 1–13

Contents lists available at ScienceDirect

Electronic Journal of Biotechnology

journal homepage: www.elsevier.com/locate/ejbt

Research article

Miracle drink supplemented with *Lactobacillus bulgaricus* loaded-chitosan/alginate nanoparticles as a medicinal food for control of MCF7 cancer cells ☆

Kumars Jovaini [a], Seyed Amir Mohammad Mortazavian Farsani [b], Seyed Hamid Aghaee-Bakhtiari [c,d], Sahar Baniyaghoob [a,*]

[a] Department of Applied Chemistry Science and Research Branch, Islamic Azad University, Tehran, Iran
[b] Department of Food Science and Technology, Faculty of Nutrition Science and Food Technology, National Nutrition and Food Technology Research Institue, Shahid Beheshti University of Medical Sicence, Tehran, Iran
[c] Bioinformatics Research Center, Mashhad University of Medical Science, Mashhad, Iran
[d] Department of Medical Biotechnology and Nanotechnology, Faculty of Medicine, Mashhad University of Medical Science, Mashhad, Iran

GRAPHICAL ABSTRACT

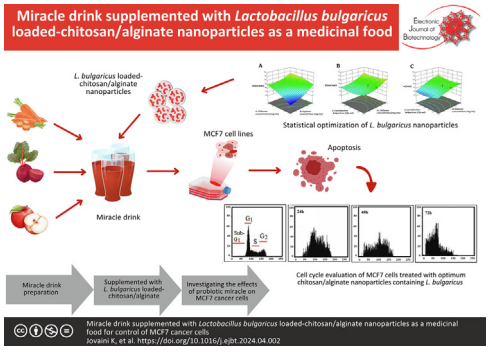

ARTICLE INFO

Article history:
Received 4 July 2023
Accepted 1 April 2024
Available online 13 May 2024

Keywords:
Alginate nanoparticles
Apoptotic effect
Cancer cells
Cancer therapy
Chitosan nanoparticles
Lactobacillus bulgaricus
Medicinal food
Miracle drink
Probiotic drink

ABSTRACT

Background: Cancer continues to be one of the greatest challenges in modern medicine and is second only to cardiovascular disease as the main cause of death. Breast cancer in particular is responsible for 15% of deaths in women. In this study, *Lactobacillus bulgaricus* was microencapsulated using a chitosan/alginate mixture. Parameters such as chitosan, alginate, and *L. bulgaricus* populations were optimized using Design Expert software. The responses were loading efficiency, particle size, release, and ζ-potential. Subsequently, the cytotoxicity of the optimized ratio of chitosan/alginate nanoparticles was investigated on MCF-7 cancer cells.

Results: The research revealed that optimal conditions for the mentioned variables were a chitosan concentration of 1% w/w, an alginate concentration of 1% w/w, and a *L. bulgaricus* count of 8.15 CFU/ml. Following numerical optimization, the loading efficacy = 91.15%, the release = 71.55%, the polydispersity index = 0.11, and the ζ-potential = 61.94 based on numerical optimization. Findings revealed that miracle drinks with *L. bulgaricus-loaded* chitosan/alginate microcapsule ratios exhibited toxic and potential apoptotic effects on MCF-7 cancer cells. This study showed that a miracle drink prepared with the optimal ratio of probiotic nanoparticles stops cells in the S and G2/M phases.

☆ Audio abstract available in Supplementary material.

Peer review under responsibility of Pontificia Universidad Católica de Valparaíso

* Corresponding author.
E-mail addresses: baniyaghoob@srbiau.ac.ir, baniyaghoob@gmail.com (S. Baniyaghoob).

https://doi.org/10.1016/j.ejbt.2024.04.002

Conclusions: The results show that Miracle drink supplemented with *L. bulgaricus* loaded-chitosan/alginate nanoparticles has a toxic and lethal effect on MCF-7 cancer cells. This compound can be suggested and used as an alternative candidate or complementary cancer therapy.

How to cite: Jovaini K, Mortazavian Farsani SAM, Aghaee-Bakhtiari SH, et al. Miracle drink supplemented with *L. bulgaricus* loaded-chitosan/alginate nanoparticles as a medicinal food for control of MCF7 cancer cells. Electron J Biotechnol 2024;70. https://doi.org/10.1016/j.ejbt.2024.04.002.

1. Introduction

Breast cancer is a prevalent malignancy among women, ranking as the second leading cause of cancer death in American women, surpassed only by lung cancer. Statistics from the National Cancer Institute of America reveal that one in eight women will develop breast cancer, implying that nearly every American family may be touched by this disease [1]. The global incidence of breast cancer is rising, especially in low-income countries. Histologically, breast cancers may resemble other tumors; however, their clinical manifestations differ, leading to varying treatment responses [2]. This variability seems rooted in the molecular structures of these tumors. Consequently, breast cancer is categorized into four groups based on gene expression patterns: luminal, pseudo-natural, HER/neu-positive human epidermal growth factor, and neural factor/receptor [3]. Several treatments exist for breast cancer, encompassing surgery, radiation therapy, and chemotherapy [4]. Chemotherapy, which uses cytotoxic drugs to halt cancer growth, eradicate it, or prevent its spread, is instrumental in the fight against breast cancer. Employed both in the early and advanced stages, chemotherapy can extend patients' lives and postpone the recurrence of the disease [5]. Notably, the anthracyclines (like doxorubicin and epirubicin) and taxanes have enhanced patient survival rates. Various drugs are used for metastatic breast cancer, including taxanes, gemcitabine, vinorelbine, and carboplatin, each with a distinct curative mechanism [6]. About 85% of breast cancers result from internal (produced by the body's glands) or external estrogens (such as oral contraceptives and hormone therapy). Historically, most of these cancers received treatment with tamoxifen, and a 5-year regimen of tamoxifen has been shown to decrease breast cancer rates by 31% [7]. However, the emergence of tamoxifen resistance and related complications has curtailed its application. Thus, there is an evident need for novel drugs that amplify tamoxifen's efficacy while minimizing its estrogenic side effects in tamoxifen-dependent cancers [8]. Recently, complementary treatment approaches, including herbal remedies, have gained traction. Some herbal concoctions have been tested on cancer cells in culture mediums or animal models [9]. A traditional anti-cancer beverage, coined "miracle juice," blends red beetroot, apple, and carrot. This mixture contains elements akin to hemo and heteropolysaccharide with specific a-L-fructopyranose connections [10]. It also boasts galactose, xylose, mannose, and glucuronic acid. Notably, due to its potent anti-cancer compound fucoidan, this drink can deter cancer cell growth, address liver, kidney, and pancreas ailments, and even heal wounds [11]. The therapeutic effects of this elixir arise from its antioxidant substance known as fucoidan. This remarkable beverage prevents the growth and proliferation of cancer cells, courtesy of its possession of the world's most potent anti-cancer compound, fucoidan. Furthermore, it thwarts liver, kidney, and pancreatic diseases, and exhibits efficacy in wound treatment [12]. The term "probiotics" describes beneficial microorganisms that confer health advantages when consumed appropriately [13]. Since its inception in 1953, numerous benefits of probiotics have been documented, such as ameliorating ulcerative colitis, diarrhea, and various other conditions [13]. Both experimental and *in vivo* studies have underscored the anti-cancer properties of probiotics. They have been shown to suppress tumorous growths, inhibit carcinogen conversion, neutralize harmful compounds, and bolster the immune system [14]. Probiotics affect the immune system by neutralizing harmful enzymes and substances that spur cancer cell growth [15]. A significant challenge with conventional probiotics is maintaining bacterial viability under gastrointestinal conditions. Research indicates that microencapsulated probiotic bacteria exhibit superior viability to their free counterparts [16]. The anticancer effect of probiotics is to prevent the conversion of procarcinogens to carcinogens, bind and deactivate mitogenic compounds, reduce the growth of carcinogenic bacteria, reduce the uptake of mitogens, and increase the function of the immune system [7]. Studies show that probiotics can play an important role in preventing colon cancer by stimulating the body's immune system and destroying destructive and carcinogenic enzymes such as secondary bile acids and mutagenic substances produced by intestinal bacteria. It also showed that the cytoplasmic extract and peptidoglycan released by lactic acid bacteria inhibit the proliferation of cancer cells [5]. Ensuring the resilience of probiotic bacteria in food is tricky, as many factors can diminish cell viability during processing and preservation. Microencapsulation envelops cells within a protective layer, effectively shielding them from the harsh, acidic environment of the stomach and the activity of intestinal enzymes [17]. Various substances, including calcium, sodium alginate, and chitosan, are used for microencapsulation under specific conditions such as temperature, pH, pressure, and so on [18]. Alginate, derived from seaweed, is favored due to its affordability, biocompatibility, non-toxicity, and adaptability; on the other hand, it is known as an FDA-approved food additive [19,20]. Chitosan is derived through the detoxification of chitin, with the chemical formula ($C_6H_{11}NO_4$). Due to its non-toxic nature, remarkable absorption properties, capacity for natural decomposition, environmental compatibility, cost-effectiveness, and ability to effectively remove a diverse array of paints and metals, along with its rapid kinetics, and the potential for producing abundant derivatives, chitosan holds significant esteem [21]. One study explored targeting murine breast cancer with magnetic iron nanoparticles incorporating L. GG cytoplasmic fractions. The findings suggested that L. GG-Cf could be a potential treatment for murine breast cancer, and magnetic iron nanoparticles might be apt for drug delivery due to their safety and magnetic attributes [22]. In one research, the association between dietary carrot intake and breast cancer was evaluated and they found that dietary carrot intake was associated with decreased risk of breast cancer [23]. Also, the relation between Betalains as cancer chemopreventative agents was studied and they found its carcinogenesis effect on cancer cell lines [24]. So far, miracle drink has not been enriched with no probiotic bacteria and its anticancer effects and toxicity have not been investigated on any cancer cell lines, which is one of the innovative aspects of the present research. This research will further explore the synergistic effects of *Lactobacillus bulgaricus*, a probiotic bacterium encapsulated within the "miracle drink" formula, on MCF-7 breast cancer cells.

2. Materials and methods

2.1. Materials

Sodium alginate (20–40 kDa), low MW chitosan (90% deacetylation, 50–190 kDa, based on viscosity), phosphate-buffered saline (PBS), MTT (3-(4, 5-Dimethylthiazol-2-yl)-2, 5-diphenyltetrazolium bromide), and MRS were procured from Sigma-Aldrich (St. Louis, MO, USA). The Amicon® Ultra-15 centrifugal filter unit 50 kDa, calcium chloride, and dimethyl sulfoxide (DMSO) were sourced from Merck Millipore (Germany). Dulbecco's Modified Eagle Medium (DMEM) high glucose medium, penicillin–streptomycin solution 100X, and *L. bulgaricus* were obtained from Iran's PTCC (Persian Type Collection Center).

2.2. Lactobacillus bulgaricus culture media preparation

In this study, *L. bulgaricus* ATCC 11849 was purchased from PTCC (Persian Type Collection Center) of Iran. The bacteria were cultured in 20 ml MRS liquid medium at 37°C for 48 h under anaerobic conditions inside an incubator (Model XB032, France-ETUVES). Post-growth, the samples underwent a rinse with sterile physiological serum and were incubated at 37°C for an additional 2 h, followed by centrifugation at 1500 rpm for 15 min. The resulting sediment was then suspended in sterile physiological serum. Concentrations were adjusted using McFarland's standard tubes to reach 2.4×10^9 CFU/ml [22].

2.3. Experimental design

The Box-Behnken design was employed to ascertain the optimal conditions for nanoparticle production. Factors such as chitosan concentration, alginate concentration, and *L. bulgaricus* population were evaluated using the Design Expert 12 software (Table 1). The interrelationship between these variables and the resulting responses was studied. Concentration ranges were represented by codes (−1, 0, and 1), denoting low, medium, and high levels, respectively. Based on preliminary experiments, the levels were set as 1 for low, 3 for intermediate, and 5 for high for chitosan and alginate. *L. bulgaricus* populations were explored in the 10^6 to 10^7 CFU/ml range.

2.4. Nanoparticles preparation

The study focused on the microencapsulation of *L. bulgaricus* using ion gelation in the two phases. Initially, 117.5 ml of a sodium alginate solution (0.063%) at pH = 4.9 was combined with a *L. bulgaricus* suspension (Table 2) and homogenized at 8000 rpm in a magnetic stirrer mixer. Subsequently, 7.5 ml of an 18 m/m calcium chloride solution was introduced to the droplet and left for 60 min until a preliminary alginate gel formed. Following this, 25 ml of a 0.07% chitosan solution, whose pH was adjusted to 6.4, was added to the pre-gel over 90 min, after 15 min. Once the chitosan was added, the mixture was left to settle for another 30 min under the previously mentioned conditions to complete the encapsulation. The nanoparticles were then isolated through centrifugation at 10,000 rpm for 30 min with PBS buffer [25].

2.5. Optimization tests of chitosan/alginate containing L. bulgaricus-loaded nanoparticles

2.5.1. Evaluation of particle size

To assess particle size, the nanoparticles were filtered using a 0.2 mm filter in distilled water containing 1% w/w Tween 80. Subsequently, their size was measured using a Zeta Sizer model (Malvern Instruments, Southborough, MA, USA) [25].

2.5.2. Investigation of nanoparticle morphology

The morphology of the nanoparticles, post-gold-coating, was studied using the FESEM Mira-Xmu model [26].

2.5.3. Loading efficiency of L. bulgaricus

To determine the amount of *L. bulgaricus* entrapped within the nanoparticles, 30 mg of the dried nanoparticles were dissolved in 25 ml of PBS buffer at pH 7.4. This solution was then stirred at 1000 rpm for 6 h. After which, it was centrifuged at 12,000 rpm for 20 min at 23°C. The concentration of *L. bulgaricus* in the supernatant was then assessed using a spectrophotometer, with readings taken in the visible spectrum at 445 nm. The entrapment efficiency (EE) was calculated using the following formula [**Equation 1**] [25].

$$EE = A/B \times 100 \quad (1)$$

where A = Concentration of *L. bulgaricus* in the nanoparticles; B = Total concentration of *L. bulgaricus*.

2.5.4. Assessment of L. bulgaricus release from nanoparticles

The cumulative release (CR) pattern of *L. bulgaricus* from the nanoparticles was studied in a saline phosphate buffer. The solution was stirred at 1000 rpm, and samples were taken at 0, 30, 60, 90, and 120 min intervals. These samples were then analyzed using *L. bulgaricus* count in MRS agar medium, plotting their release profiles over time. The cumulative release percentage at each interval was calculated by adding the *L. bulgaricus* count in each interval to the preceding interval's value [**Equation 2**] [25].

$$\frac{dMt}{dt} = k\text{Zero} - \text{degree equation} \quad (2)$$

where k represents a constant, t is the time, and M_t is the quantity of *L. bulgaricus* released at the time t. M and M_0 denote the release quantities at the beginning (time zero) and at the time t,

Table 1
Variables used in Box-Behnken design.

Dependent variables	Symbol	Level		
		−1	0	1
X1 = Chitosan concentration	A	1	2.52.5	5
X2 = Alginate concentration	B	1	2.5	5
X3 = *Lactobacillus bulgaricus* population	C	10^6	$10^{5.5}$	10^7
Dependent variables	**Units**	**Constraints**		
Y1 = Nanoparticles size (NS)	nm	Minimum		
Y2 = Polydispersity index (PDI)	–	<0.05		
Y3 = ζ-potential	mV	Max		
Y4 = Loading efficacy (LE) (%)	%	Max		
Y5 = Cumulative release (CR)(%)	%	Max		

Table 2
Box–Behnken design matrix and results of experiments.

		Factor 1	Factor 2	Factor 3	Response 1	Response 2	Response 3	Response 4	Response 5
Std	Run	A: Chitosan concentration mgr/ml	B: Alginate concentration mgr/ml	C: *L. bulgaricus* cfu/ml	Size nm	Loading efficacy %	Release %	PDI	ζ-potential mv
1	1	1	1	1E+0.6	566	75	55	0.63	42
2	2	5	1	1E+0.6	512	71	51	0.6	47
9	3	0.363586	3	5.5E+0.6	566	75	55	0.63	47
10	4	6.36359	3	5.5E+0.6	534	69	48	0.61	44
13	5	3	3	2.06807E+0.6	723	40	20	0.8	35
16	6	3	3	5.5E+0.6	343	89	69	0.43	55
8	7	5	5	1E+0.7	511	71	51	0.5	42
4	8	5	5	1E+0.6	534	69	49	0.52	42
18	9	3	3	5.5E+0.6	233	95	75	0.1	60
14	10	3	3	1E+0.7	212	85	65	0.1	64
20	11	3	3	5.5E+0.6	788	50	30	0.8	35
3	12	1	5	5.5E+0.6	712	55	35	0.8	32
15	13	3	3	5.5E+0.6	414	74	54	0.4	51
19	14	3	3	5.5E+0.6	412	74	54	0.4	51
5	15	1	1	1E+0.7	512	71	51	0.5	47
11	16	3	0.363586	5.5E+0.6	589	70	50	0.55	42
7	17	1	5	1E+0.7	411	74	54	0.4	52
12	18	3	6.36359	5.5E+0.6	411	74	54	0.4	52
17	19	3	3	5.5E+0.6	411	74	54	0.4	52
6	20	5	1	1E+0.7	411	74	54	0.4	52

respectively. Differentiating the above [**Equation 3**] and [**Equation 4**] yields:

$$\frac{dMt}{dt} = K(M0 - Mt)\text{First} - \text{class equation} \quad (3)$$

$$1 + 2F - 3F^{3/2} = Kt \qquad F = 1 - Mt/M^{\infty}\text{Higuchi Model} \quad (4)$$

2.5.5. Statistical optimization of chitosan/alginate nanoparticles loaded with L. bulgaricus

The optimal condition was ascertained through numerical optimization after conducting nanoparticle experiments, with results provided in (Table 1). The software evaluated the predicted point, and it was replicated seven times. Once the observed and predicted values aligned, this optimal formula was implemented to create the functional drink [23].

2.5.6. Culture of MCF7 cancer cells

MCF7 carcinoma cells (PN = 1) were obtained from the Genetic Resources Center (GRC) in Iran. A flow cytometry test was conducted to validate breast cancer markers, specifically HER-2, utilizing the facilities of the Genetic Resource Center of Iran. The cells were cultivated in a 25 ml flask, with the culture medium comprising RPMI 10% (GIBCO, USA), FBS, 2 ml glutamine, 100 U/ml^{-1} penicillin, and 100 mg/ml streptomycin. Subsequently, the flask was placed in an incubator at a temperature of 37°C. Following a 72 h period, the cells underwent passaging to acclimate to their surroundings and facilitate growth. The process of cell passaging employed 1X trypsin [24].

2.5.7. Cell viability assay via MTT method for the probiotic miracle drink

The MTT assay was carried out employing the tetrazolium dye. An MTT solution of 5 mg/ml concentration was prepared in deionized water. After 24 and 48 h, cell groups, each containing 20,000 cells/well, were cultured. These plates were incubated for 24 h. Subsequently, the remaining medium was decanted, and 100 µl of dimethyl sulfoxide (DMSO) was added to every well until formazan crystals dissolved. Post plate agitation for 10 min, the optical density of formazan was gauged at 570 nm using a plate reader [26].

2.5.8. Assessment of functional beverage impact on MCF-7 cancer cell lines

MCF-7 human breast cancer cells were cultivated in T75 flasks, with the population set at 5,000 cells/well. These were grown in low glucose Dulbecco's modified Eagle's medium (DMEM) enriched with 10% fetal bovine serum (FBS), 2 mM glutamine, 0.01 mg/ml insulin, and 1% penicillin/streptomycin mix. These cells were incubated at 37°C under 5% CO2 and permitted to adhere to the flask base. After 2 h of incubation, the cellular morphology was placed inside the incubator for 2 h morphological condition of the cells, the different treatments were assessed: miracle drink (T1), miracle drink infused with probiotic nanoparticles (T2), probiotic nanoparticles alone (T3), and positive control of cells in culture medium devoid of any treatment. The experiments were conducted in triplicates (T). The cancer cell proliferation was monitored for up to 72 h, and a growth trajectory for these cells was plotted [27].

2.5.9. Analysis of treated MCF-7 cancer cell cycle

Cells treated with the miracle drink underwent stabilization using 70% ethanol for 2 h of a PI master mix solution, comprising 40 µl of propidium iodide, RNase, and 950 µl of saline phosphate buffer. The mixture was incubated at 37°C for 30 min. Subsequently, flow cytometry analysis was performed, and the resulting data were examined using Flow Jo 7.6.1 software [27].

2.5.10. Assessment of apoptosis by Hoechst staining

This method cultured 2×10^5 cells/well in two 24-well plates. The first was well-acted as a control, while the second was treated with an IC50 concentration of the Embelin compound. After an incubation period of 72 h, cells from each well were centrifuged. A total of 200 µl of methanol was then introduced to the cell sediment and stored at −20°C for 20 min to fix the cells. Following another centrifugation, 100 µl of the cell suspension in saline phosphate buffer, containing 1 µl of Hoechst 3342, was incubated at room temperature for 30 min. After a final centrifugation, the cell pellet was resuspended, and the mixture was incubated at 25 ± 1°C for 30 min. Finally, 50 µl of saline phosphate buffer was added to the cell mixture, and a 10 µl sample of this was placed on a microscopic slide for observation under a fluorescence microscope (Olympus) [28].

3. Results and discussion

3.1. Size of probiotic nanoparticles

Based on the analysis in Table 2, a secondary relationship was identified between the nanoparticle size and the research variables, with a correlation coefficient of R^2 = 0.88. As anticipated from the experimental results, chitosan and alginate concentrations significantly impacted nanoparticle size ($p \leq 0.05$). However, bacterial concentration did not substantially affect the size of nanoparticles ($p > 0.05$).

[**Equation 5**] represents the relationship as follows:

$$NS = +435 + 109.76A + 106.18B - 0.3868C - 35.87AB + 1.25AC + 28.44BC + 5414A^2 - 31.40B^2 + 45.88C^2 \quad (5)$$

where: *A* represents chitosan concentration, *B* denotes alginate concentration, and *C* is for *L. bulgaricus* concentration (Fig. 1).

It was observed that nanoparticle size increased with a rise in chitosan concentration. As chitosan concentration escalates, the viscosity of the solution grows, thereby elevating the liquid's resistance to dispersion, which results in larger particles. Furthermore, as the concentration of chitosan increases, its molecules come closer, leading to coalescence and dispersion of tri-polyphosphate molecules within the chitosan molecule. This results in the formation of larger particles. Comparable findings were reported by Karimi Ziadashti et al. [26], who explored chitosan nanoparticles for targeted drug delivery. Similarly, Budi et al. [28] emphasized the role of chitosan concentration in determining nanoparticle size. Significantly reducing the alginate concentration diminishes the size of calcium alginate nanoparticles drastically. This change is attributed to the fewer polymer chains of sodium alginate, leading to a subsequent reduction in attached carboxylate ions and ether and hydroxyl groups to calcium ions. With a decrease in functional groups surrounding calcium ions, fewer alginate chains interact in this process, thereby diminishing the average size of these particles. Conversely, an increase in alginate concentration yields a noticeable augmentation in particle size. Sarei et al. [29] underscored the significant impact of alginate concentration on nanoparticle size and they observed similar results in agreement with our research. Regarding bacterial concentration, different levels did not significantly influence nanoparticle size ($p \leq 0.05$). This phenomenon can be attributed to the stoichiometric ratio governing the reaction between the positively charged ions of chitosan and the negatively charged ions of alginate. As a result, a precise percentage of bacteria becomes encapsulated within the ion network. Thus, the bacteria remain entrapped within the formed network when determining particle size. Oberoi et al. [30] reported similar findings, wherein no significant relationship was observed between probiotic quantity and hydrogel size.

3.2. Loading efficacy of L. bulgaricus

The analysis of variance presented in Table 2 reveals a secondary correlation between loading efficacy and the research variables, denoted by an R^2 = 0.9785. The experimental results, as anticipated, highlight the significant impact of chitosan and alginate concentrations on the loading efficiency of *L. bulgaricus* ($p \leq 0.05$). Conversely, the concentration of bacteria about loading efficacy did not exhibit significance ($p \leq 0.05$). Notably, the mathematical model integrating chitosan and alginate concentrations and particle size [**Equation 6**] underscores a marked reduction in loading efficacy associated with the negative coefficient of variation ($p \leq 0.05$). The absence of a fit index value further implies that, apart from the three variables studied, additional variables need not be incorporated to model changes in loading efficiency within the formulation components.

[**Equation 6**] represents the relationship as follows:

$$LE = +73.04 - 9.48A - 8.87B + 0.0567C - 0.7500AB - 1.67AC - 2.21BC - 5.75A^2 + 5.16B^2 - 1.16C^2 \quad (6)$$

where: *A* represents chitosan concentration, *B* denotes alginate concentration, and *C* is for *L. bulgaricus* concentration (Fig. 2).

Encapsulation, encompassing the confinement of valuable bioactive compounds within an appropriate carrier, fosters microcapsule stability. The encapsulation material or compound within the capsule can be transferred through dissolution, entrapment, absorption, or binding within the matrix [30]. This study underscores that elevating chitosan and alginate concentrations in chitosan/alginate microcapsule formulation directly correlates with a notable reduction in *L. bulgaricus* trapping. This reduction can be attributed to the increased molecular weight of polymers within the formulation, leading to an imbalance in positive and negative charges and stoichiometry. Notably, loading efficiency significantly diminishes when concentrations surpass 1% [31]. With chitosan bearing a positive charge, its interaction with the negatively charged alginate neutralizes its electrical charge. However, augmenting the *L. bulgaricus* population within the whey protein and alginate balance formulation does not yield complete microemulsion formation, leading to a considerable decrease in equilibrium. The release of nanoparticles is influenced by diverse factors, with hydrolysis as a key degradation mechanism [28]. This process involves the reaction between water molecules and bonds within the polymer chain, releasing trapped compounds [26]. Zohri et al. [32], in their study of bone morphogenetic protein-2 trapping in chitosan/alginate nanoparticles, also came to similar conclusions regarding the relationship between nanoparticle size and the ability to release and trap. They found that as the size of the nanoparticles increased the release decreased significantly [32].

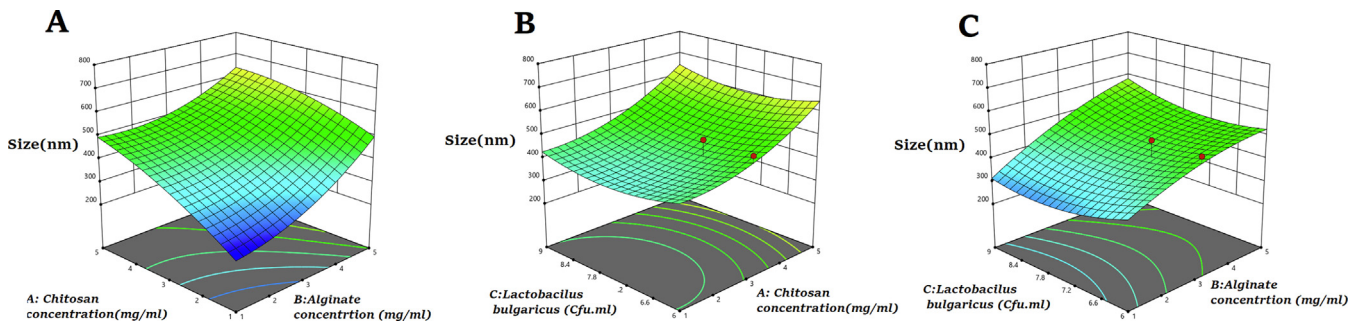

Fig. 1. 3D Response surface plots (A-C) for the mean of nanoparticle size and relationship between chitosan concentration, alginate concentration, and *L. bulgaricus*. It graphs two predictor variables, X and Y, on the y-axis and a response variable.

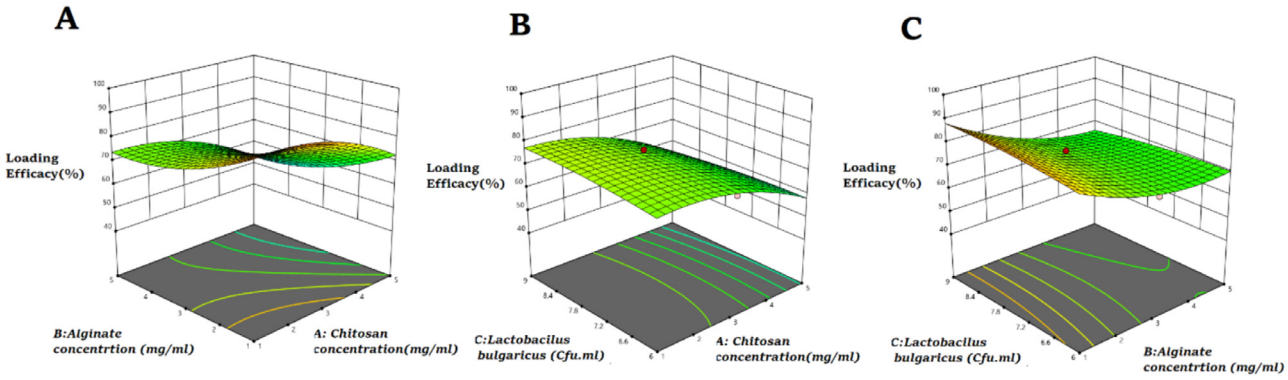

Fig. 2. 3D Response surface plots (A-C) for the mean of nanoparticles loading efficacy and relationship between chitosan concentration, alginate concentration, and *L. bulgaricus*. It graphs two predictor variables, X and Y, on the y-axis and a response variable.

3.3. The cumulative release of L. bulgaricus

The variance analysis in Table 3. indicates a second-order relationship between release and research variables, as evidenced by a correlation coefficient of R^2 = 0.9778. The impact of chitosan and alginate concentrations on the release of *L. bulgaricus* is pronounced ($p \leq 0.05$).

Fig. 3. demonstrated that by increasing the concentration of chitosan and alginate, the release percentage of L. casei decreases significantly, which has a negative and significant relationship with the increase in particle size of microcapsules, and because this increase in the concentration of chitosan and alginate up to 5%, causes increase polymer particles are suspended in the environment and these particles reduce the contact area of the particles by increasing the degree of crosslinking and the creation of agglomeration that reduces the release of bacteria. Undoubtedly, the higher the agglomeration of particles, the lower the release. However, the percentage of entrapped probiotic bacteria decreased with increasing chitosan and alginate concentration, and the percentage of release also followed the same pattern and decreased with increasing chitosan and alginate concentration. On the other hand, the same stoichiometric ratios are necessary to obtain particles with a smaller size [33]. Many factors also affect the release rate of nanoparticles. Most of the biodegradable polymers used in microemulsion systems are degraded by hydrolysis. Hydrolysis is a reaction between water molecules and bonds in the main polymer chain. An example of these bonds is the ester bond. When they are broken one after the other, the polymer chain is broken down into its monomers. When the water molecules break the chemical bonds along the molecular chain, the physical cohesion of the polymer is broken, allowing the trapped compound to be released [34]. The release kinetics of probiotic bacteria from chitosan/alginate nanoparticles is described in two phases of the biphasic process. The initial stage consists of initial bursting which causes slow release in chitosan/alginate nanoparticles [35]. In higher counts of *L. bulgaricus* (accumulation rate above 50%), it takes about 1 h for this initial release to take place. In accumulations with a lower percentage and the presence of unloaded *L. bulgaricus* in the environment, the process has become a one-step process with an increase. The count of *L. bulgaricus* entrapment, the amount of entrapment and finally the amount of release increases. One of the factors affecting the release rate of *L. bulgaricus* is the size of the nanoparticles, which effectively reduces the contact surface of the nanoparticles by increasing the size of the nanoparticles, which can reduce the release rate of compounds trapped inside the nanoparticles [36]. Heightened concentrations of chitosan and alginate lead to a significant reduction in *L. bulgaricus* release. This reduction can be attributed to the augmented mass of suspended polymers within the environment due to increased concentrations, leading to heightened interconnection and agglomeration, ultimately hampering bacteria release [37]. The inverse relationship between agglomeration rate and release magnitude is evident. Concurrently, higher chitosan and alginate concentrations lead to decreased entrapment efficacy of probiotic bacteria, aligning with the pattern of reduced release. Moreover, maintaining stoichiometric equilibrium is pivotal for achieving smaller particle sizes [34]. This decline is most pronounced when chitosan and alginate concentrations and the entrapment efficacy of probiotic bacteria decrease. The reduction of release followed the same pattern and thus decreased with increasing chitosan and alginate concentrations and particle size [**Equation 7**] further accentuating the reduction in release ($p \leq 0.05$).

Equation 7 represents the relationship as follows:

$$CR = +5306 - 9.88B - 0.525C - 0.7500AB - 1.67AC - 2.21BC - 5.72A^2 + 5.20B^2 - 1.31C^2 \quad (7)$$

where: *A* represents chitosan concentration, *B* denotes alginate concentration, and *C* is for *L. bulgaricus* concentration.

The release of nanoparticles unfolds across three distinct stages: the initial release or first phase, the solid release phase, and the degradation phase [35]. Additionally, various factors influence nanoparticle release rates. Hydrolysis emerges as the primary degradation mechanism for most biodegradable polymers within microemulsion systems, involving the reaction between water molecules and polymer chain bonds [36]. This process culminates

Table 3
Analysis of variance for Box–Behnken design refined models.

Dependent variables	Source of variations	Mean square	F-value	P-value > F	R^2	Adjusted R^2	Predicted R^2
Nanoparticles size	Model lack of fit	41203.46	8.25	0.0014	0.0014	0.7745	0.1715
Loading efficacy	Model lack of fit	309.31	50.6	< 0.0001	0.9785	0.9592	0.8381
Cumulative release	Model lack of fit	309.72	48.88	< 0.0001	0.9778	0.9578	0.8336
Polydispersity index	Model lack of fit	0.0636	4.51	0.0138	0.8023	0.6244	−0.1299
ζ-potential	Model lack of fit	125.93	8.88	0.001	0.8888	0.7887	0.2184

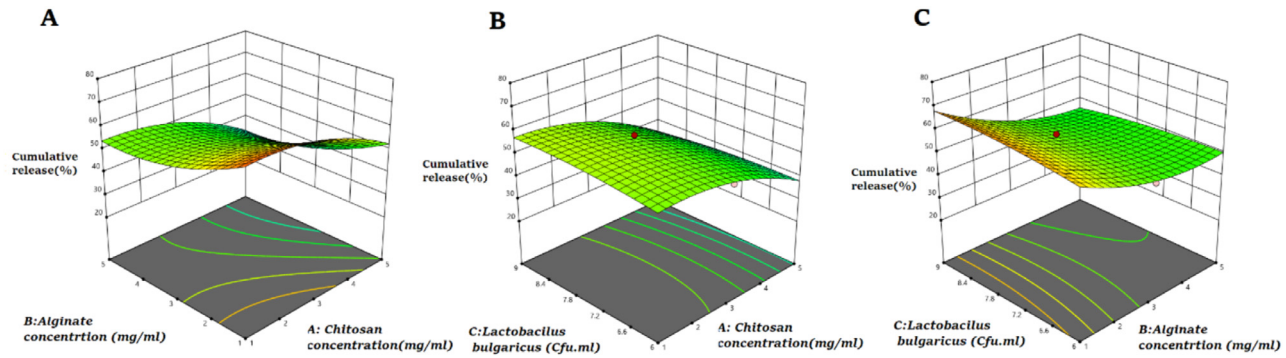

Fig. 3. 3D Response surface plots (A-C) for the mean of nanoparticles cumulative release and relationship between chitosan concentration, alginate concentration, and *L. bulgaricus*. It graphs two predictor variables, X and Y, on the y-axis and a response variable.

in the release of trapped compounds, disrupting the physical integrity of the polymer. The release kinetics of probiotic bacteria from nanoparticles adhere to a biphasic pattern, encompassing an initial burst phase that subsequently leads to gradual nanoparticle release [37]. This initial release phase typically spans one hour, with environments featuring lower percentages of probiotic bacteria witnessing a halt. However, the augmented loading efficacy of probiotic bacteria correlates with increased release rates [38]. Notably, microcapsule size plays a pivotal role in this phenomenon. Larger nanoparticles exhibit diminished contact effectively areas, contributing to reduced release of entrapped compounds. Consequently, the results presented here affirm the considerable influence of trap index size [34]. In one research, Dimitrellou et al. [37] studied the encapsulation of *Lactobacillus casei* ATCC 393 in alginate capsules for probiotic fermented milk production and found that the concentration of each of the three compounds was increased, when, which was consistent with the findings of the present study.

3.4. Polydispersity index

After a thorough analysis of the variance presented in Table 3, it was determined that a second-order relationship exists between the polydispersity index and the research variables, demonstrating an impressive $R^2 = 0.9778$. The results from the variance analysis in Table 3 indicated a significant impact of chitosan concentration and alginate on the polydispersity index of *L. bulgaricus* ($p \leq 0.05$). Notably, based on (Fig. 4), increasing the chitosan and alginate concentration led to a substantial decrease in the polydispersity index. This decrease is intrinsically tied to a negative and significant correlation with the enlargement of microcapsule particle size. Notably, the augmentation of chitosan and alginate concentrations up to 5% contributes to an enlargement of suspended polymers within the environment. Consequently, these particles facilitate heightened crosslinking and agglomeration, reducing particle contact area [38]. This diminution in particle contact area subsequently contributes to diminished microcapsule stability and an increased polydispersity index. Research has consistently indicated that heightened particle agglomeration corresponds to escalated instability and a substantially reduced polydispersity index [30]. The positive coefficient signifying changes in chitosan and alginate concentrations within the mathematical formulation model [**Equation 8**] corroborates this finding by indicating a rise in polydispersity with increasing concentrations of chitosan and alginate ($p \leq 0.05$). Furthermore, the absence of a contestability index implies no imperative need to introduce additional variables (beyond the three variables under study) to account for changes in the polydispersity index about formulation components.

Equation 8 represents the relationship as follows:

$$PDI = +0.4540 + 0.1495A + 0.1216B - 0.0134C - 0.0636AB + 0.0002AC + 0.0261BC + 0.049A^2 - 0.0408B^2 + 0.0433C^2 \quad (8)$$

where: *A* represents chitosan concentration, *B* denotes alginate concentration, and *C* is for *L. bulgaricus* concentration.

As illustrated in Fig. 4, the polydispersity index experiences a noticeable increase with the augmentation of particle size, chitosan, and alginate concentrations exceeding 3%. This trend underscores a reduction in nanoparticle stability. The polydispersity index, also called the dispersion index, encapsulates the average molecular weight ratio to the mean molecular weight. Approach-

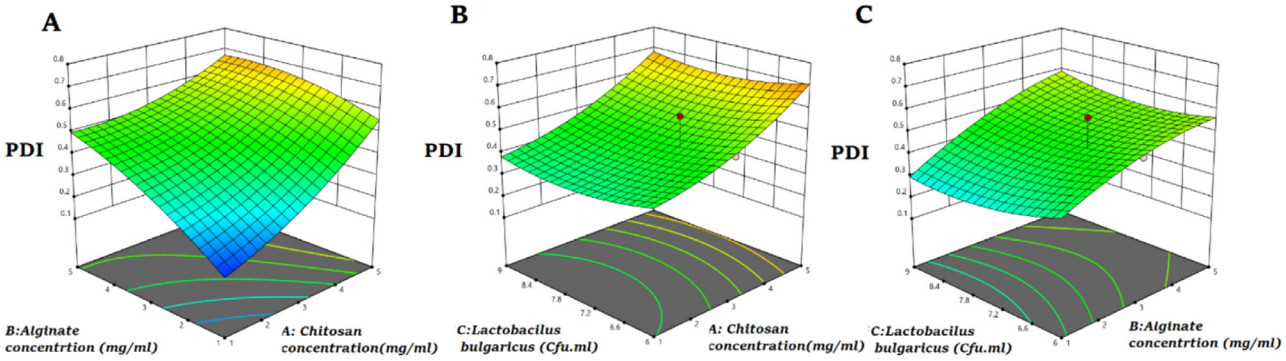

Fig. 4. 3D Response surface plots (A-C) for the mean of nanoparticles Polydispersity Index (PDI) and the relationship between chitosan concentration, alginate concentration, and *L. bulgaricus*. It graphs two predictor variables, X and Y, on the y-axis and a response variable.

ing a ratio of one enhances the elevation of the chart. This phenomenon has been extensively documented [34]. The polydispersity index is a pivotal gauge of stability and uniformity, with dimensions, particle type, and pH exerting significant influence. A rise in the molecular weight ratio of chitosan/alginate introduces an imbalance between the positively charged chitosan molecules, negatively charged alginate molecules, and unbound chitosan molecules. This imbalance curtails the likelihood of interactions between chitosan, alginate, and *L. bulgaricus*, resulting in augmented nanoparticle size and ζ-potential while diminishing homogeneity [38]. Parallel inquiries have corroborated these findings. A study investigating the impact of chitosan/alginate encapsulation with inulin on *Lactobacillus rhamnosus* survival during apple juice storage under digestive conditions concluded that higher molecular weight chitosan and alginate led to increased polydispersity, thereby reducing instability rates [30]. Another examination delved into the stability of microencapsulated *L. bulgaricus* YIT 9018 using chitosan and alginate, affirming the pivotal role of chitosan and alginate concentrations in microcapsule stability, aligning seamlessly with our current study's findings [39]. Similarly, an investigation centered around alginate and chitosan microgels for microencapsulation corroborated our findings by indicating an upswing in instability and polydispersity index with heightened polymer concentrations [20].

3.5. ζ-Potential index

Upon scrutiny of the variance analysis provided in Table 3, it becomes evident that the relationship between the ζ-Potential index and the research variables adheres to a second-order pattern, with a commendable R^2 = 0.9778. According to Table 3, the influence of chitosan and alginate concentrations on the lactobacillus bulgaricus polydispersity index is noteworthy ($p \leq 0.05$). Delving into Table 3 and Fig. 5 reveals a substantial decrease in the ζ-Potential index of nanoparticles with escalating polymer concentrations ($p \leq 0.05$). The dimensions and distribution of colloidal systems, whether uniform or non-uniform, exert significant control over their characteristics. The sustained constancy of these parameters over an extended timeframe is a reliable indicator of system stability. The affirmative coefficient associated with changes in chitosan and alginate concentrations within the mathematical model for formulation components and the ζ-Potential index [**Equation 9**] signifies a heightened ζ-Potential through heightened chitosan and alginate concentrations ($p \leq 0.05$). The absence of a fit index logically indicates the redundancy of introducing supplementary variables (beyond the triad of variables studied) into the model governing ζ-Potential alterations for formulation components.

Equation 9 represents the relationship as follows:

$$\zeta - \text{Potential} = +50.74A - 6.37A - 4.86B + 0.0561C + 2.25AB + 1.04AC - 2.85A^2 + 1.45B^2 - 3.15C^2 \quad (9)$$

where: *A* represents chitosan concentration, *B* denotes alginate concentration, and *C* is for *L. bulgaricus* concentration.

The ζ-Potential stands as a functional facet of membrane surface electrical charge. Factors such as the cellular environment, ion concentration, and environmental pH wield discernible influence over the ζ-Potential. Enlargement of particle size and subsequent formation of larger aggregates can profoundly impact surface loads and ζ-Potential reduction [40]. This phenomenon can be attributed to the neutralization of surface charge, particle agglomeration, and the creation of bridges between adjacent particles. Particle cohesion, facilitated by an absorptive reaction between particles carrying opposite charges, is particularly pronounced at ambient temperatures. This process culminates in the agglomeration of microcapsules, yielding clusters that augment particle size and heterogeneity [33]. Consequently, larger particles experience a marked reduction in ζ-Potential magnitude compared to their smaller counterparts. Pertinent studies resonate with these findings, further validating their robustness.

3.6. Statistical optimization and validation

The response surface methodology was employed using Design-Expert® software (Trial version 12; Stat-Ease Inc., Minneapolis, MN, USA) to optimize the preparation conditions of chitosan/alginate nanoparticles containing *L. bulgaricus*. Within this method, the correlation between responses and variables was also explored. For optimization, the Box-Behnken design was employed. The non-independent variables (pH, stirring rate, and molecular ratio of chitosan/alginate) and their impact on responses (considered as non-independent factors), which encompass particle size (Y1), loading efficacy (Y2), cumulative release (Y3), ζ-potential (Y4), and polydispersity (Y5), were investigated. The range of concentrations within the (−1, 0, 1) intervals, representing low, medium, and high levels, respectively, was determined based on preliminary experiments conducted during nanoparticle production and studies to optimize chitosan/alginate microcapsules. Upon analyzing the outcomes, the optimal values of 1 for chitosan concentration, 1 for alginate concentration, and a *L. bulgaricus* concentration of 8.15 cfu/g were selected.

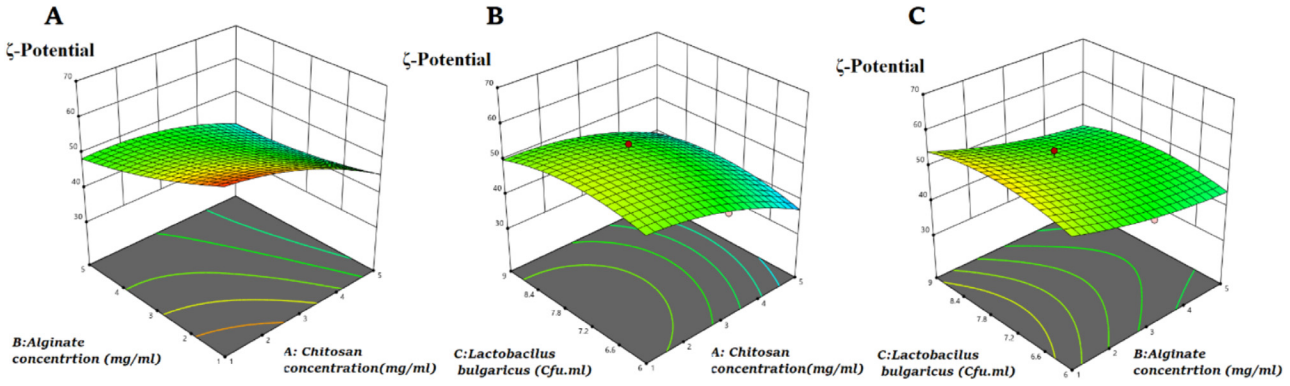

Fig. 5. 3D Response surface plots (A-C) for the mean of nanoparticles ζ-Potential and the relationship between chitosan concentration, alginate concentration, and *L. bulgaricus*. It graphs two predictor variables, X and Y, on the y-axis and a response variable.

3.7. Morphology of microcapsule loaded with L. bulgaricus with optimized ratio

The microcapsule morphology is illustrated in Fig. 6. The image shows that the nanoparticles exhibit a uniform, non-agglomerated appearance with a soft texture. The average particle size was measured between 150–200 nm.

3.8. Analysis of cancer cell growth and cytotoxicity

Based on Fig. 7, it was observed that the population of cancer cells increased over time. However, the growth rate was lower in the probiotics-treated group compared to the control. The findings revealed that nanoparticles hindered the growth of MCF7 cancer cells compared to the control treatment. This effect depended on the dosage of nanoparticles containing *L. bulgaricus* and the duration of exposure. As the concentration increased within the specified timeframe, the inhibition of cancer cells also increased. Consistently, Fig. 7 demonstrated a similar trend in the viability of MCF-7 cancer cells from 2 to 4. During this period, they also exhibited cytotoxicity and cell survival changes. Moreover, the rate of cell death exhibited a notable rise in the exposure time, and viability duration increased. This heightened toxicity was most prominent at the highest dosage of the probiotic miracle drink.

Fig. 8 displayed a comparable pattern concerning the viability of MCF-7 cancer cells. Moreover, significant cytotoxicity was evident between the different cancer cell treatments ($p \leq 0.05$). The cell death rate also experienced a significant increase with increasing marked elevation as the duration of exposure and viability extended. This enhanced toxicity was most evident at the highest dosage of the probiotic drink. The more significant toxicity towards cancer cells can be attributed to multiple factors. Firstly, cancer cells display a heightened activity of mitochondria in their respiratory process compared to normal cells. This disparity creates favorable conditions for bacterial cell components to target and eliminate cancer cells [41]. Additionally, morphological distinctions between normal and cancerous cells and variations in cellular pores may contribute to the observed cytotoxicity. Numerous studies have delved into the cytotoxic effects of probiotics on cancer cell lines. Chen et al. [42] investigated the impact of probiotic lactobacillus on the growth of human colonic carcinoma cell line HT-29. The researchers revealed that components from heat-treated bacterial cells, including cell walls, peptidoglycans, and cytoplasm, exert cytotoxic effects on cancer cells [43]. Similarly, Er et al. [44] explored the cytotoxicity of different Lactobacilli strains on Caco-2 cancer cells, indicating that extracts from Lactobacilli bacterial strains hindered cancer cell growth dose-dependent. One of the reasons for the heightened toxic effects on cancer cells is the heightened activity of mitochondria in the respiration process of cancer cells, as compared to normal cells. These conditions provide a suitable environment for the composition of bacterial cells capable of targeting the destruction of cancer cells. Another contributing factor is the morphological disparity between normal and cancer cells and variations in the number of cellular cytoplasmic pores. This aspect can further substantiate the observed cytotoxicity [45]. Numerous studies have explored the cytotoxic effects of probiotics on cancer cell lines. A study by Er et al. [44] investigated the cytotoxic effects of different Lactobacilli bacteria on Caco-2 cancer cells bacterial strains of *L. bulgaricus* were found to reduce the survival rate of HT29 and Caco-2 cancer cells. These researchers demonstrated that various cellular components of heat-treated bacteria, such as cell walls, peptidoglycans, and cytoplasm, all exert cytotoxic effects on cancer cells [44]. This study also indicated that the extract from Lactobacilli bacterial strains inhibits the growth of cancer cells in a dose-dependent manner, which aligns with the current study's findings. The cell extracts of *L. bulgaricus* were observed to inhibit cancer cells in a dose-dependent manner. Inducing programmed cell death is a fundamental approach in cancer treatment. Cell death pathways encompass a series of proapoptotic events within the cell, commencing with the Bax and Bak proteins' permeabilization of the mitochondrial outer membrane. This process leads to the release of cytochrome *c*, subsequently activating caspase 9 and then caspase 3 [23]. Additionally, Bcl2 and Bcl-xl proteins on the surface of the endoplasmic reticulum hinder the interaction between Bax and Bak proteins, exhibiting anti-apoptotic activity. In this study, the encapsulation of *L. bulgaricus* was achieved using chitosan. Chitosan is a natural polymer with unique properties such as water absorption, controlled release, and bio-mineralization. Its derivatives, such as carboxymethyl chitin and hydroxypropyl chitin, possess immunomodulatory effects, enhancing both innate and acquired immunity. This augmentation increases cell activity, cytokine, and chemokine secretion [40]. Notably, chitin and its derivatives are absent in the human body's structure; their presence is an immune system activator. Receptors like detection-1, TLR-2, and mannose receptors are accountable for recognition and subsequent activation. Chitosan suspensions and particles are proficient in stimulating the immune system through mechanisms like chemotaxis and macrophage activation, which leads to the release of inflammatory cytokines. This polymer amplifies antibody response cytotoxic T cell activity and also triggers natural killer cells. Significantly, chitosan exhibits lower toxicity levels in normal cells [43]. Among the pathological responses is the infiltration of neutrophils, lymphocytes, and macrophages, which are sources of pro-inflammatory cytokines and reactive oxygen species (ROS). Furthermore, fibroblasts migrate to the lesions, introducing bioactive components like betaine, polyphenols, carotenoids, flavonoids, and saponins. Water-soluble pigments like betalain from red beetroot, carrot, and apple exhibit anti-mutagenic properties against the direct-acting mutagen Methyl nitro-nitrosoguanidine (MNNG). The outcomes of this research also corroborate that the "miracle drink" exerts an anti-cancer influence on MCF-7 cells over 72 h, leading to a substantial decrease in the MCF-7 cell population [46]. The utilization of nanoparticles has the potential to enhance the anti-cancer and toxicity effects by promoting the viability of probiotic bacteria. Due to their robust antioxidant properties and

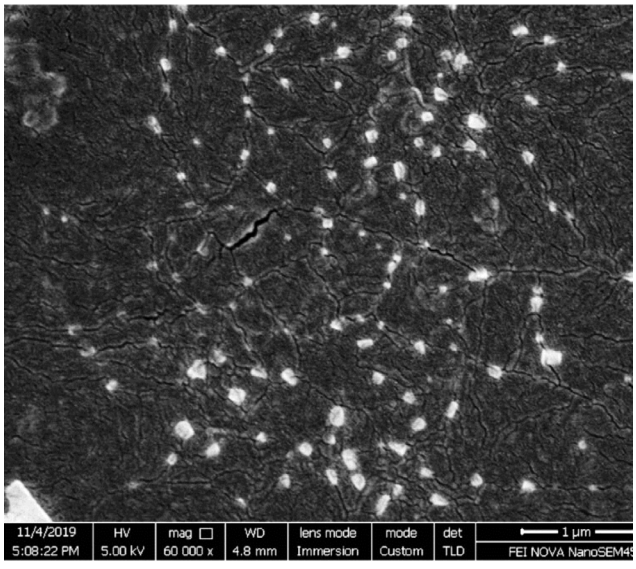

Fig. 6. Morphology of optimum formulation of *L. bulgaricus* loaded chitosan/alginate nanoparticles. The scale bar is 1 µm.

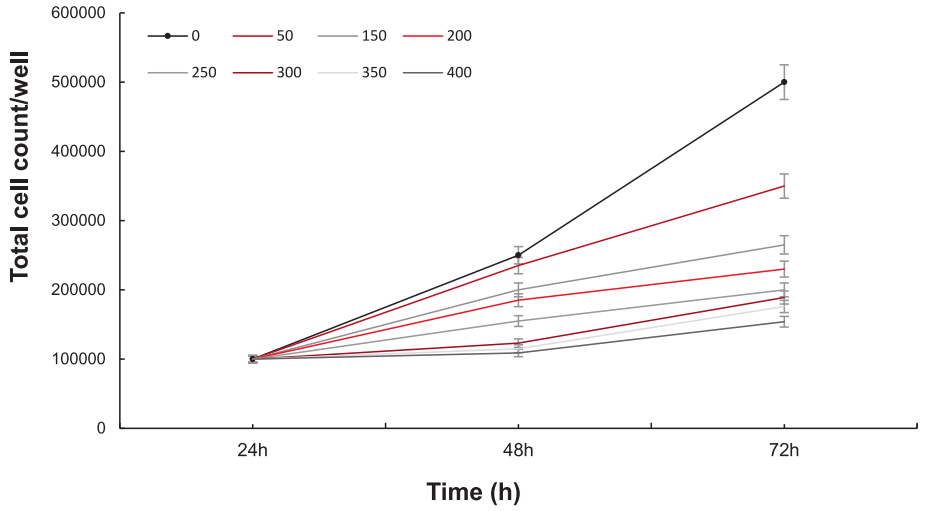

Fig. 7. Comparison of MCF7 cell growth at intervals of 24, 48, and 72 h. Cell viability is calculated as; viability (%) = Mean OD/Control OD × 100%. All data are presented as the mean of three different measurements.

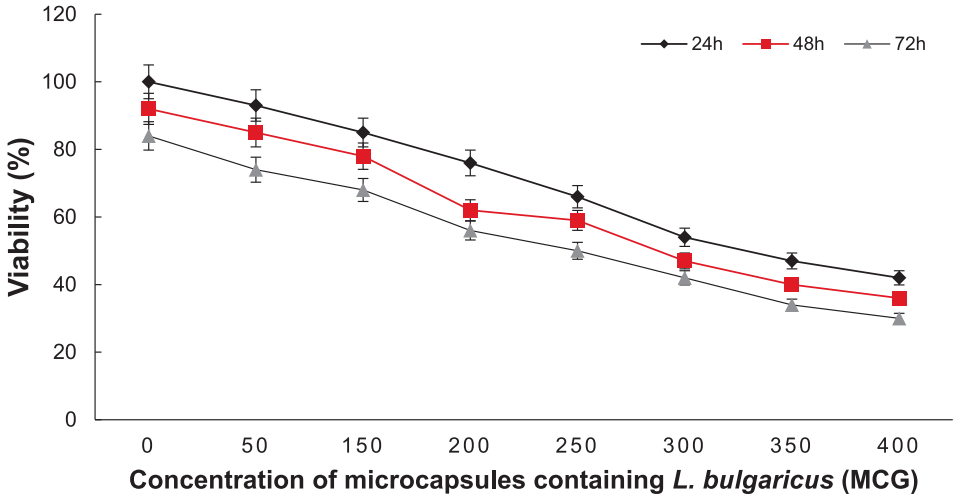

Fig. 8. Comparison of cytotoxicity of *L. bulgaricus* nanoparticles on MCF7 cells at intervals of 24, 48, and 72 h. Cell viability is calculated as viability (%) = Mean OD/Control OD × 100%. All data are presented as the mean of three different measurements.

high nutritional value, Miracle drinks can extend their shelf life, owing to their synbiotic attributes and the presence of *L. bulgaricus* [45]. Betalain, a constituent of sugar beet extract, has demonstrated anti-cancer effects in multiple studies. In a particular study, the impact of 6-methoxymeelin isolated from carrots on stem cancer cells was explored within the context of NF-κB signaling. The findings indicated that 6-methoxymeylin could be an efficacious anti-cancer agent for suppressing BCSCs using NF-κB/IL-6 and IL-8 inhibitors [43]. Consequently, due to the presence of anti-cancer compounds in the triple combination of red beet, carrot, and apple, along with microencapsulated probiotics, this product significantly retards the growth of MCF-7 cells.

3.9. Evaluation of the cell cycle of MCF-7 cancer cells

Fig. 9 illustrates the cell cycle analysis of MCF-7 cancer cells compared to the control group. The G1 phase exhibited a larger cell volume of 120% compared to other phases. Within the 24 h group, 40% of cancer cells transitioned to the S phase, while 20% entered the G2 phase. Over 48 h, a higher percentage of cell volume shifted to the G2 phase, maintaining a consistent level. At the 72 h mark, less than 10% of cells were in the G2 phase. This study demonstrates that the optimal composition of probiotic nanoparticles in the miracle drink arrests cells in the S and G2/M phases. The susceptibility of MCF-7 cancer cells to this probiotic miracle drink can be attributed to DNA strands in various stages of cell division, particularly the S phase, which becomes accessible for synthesis. The bioactive compounds, including flavonoids, betalain, and substances secreted by *L. bulgaricus*, strongly connect to DNA openings such as Intarstrand and Interastrand [47].

As a result, normal progression through the phases of cell division is disrupted, leading to diminished growth. Notably, altering the concentration of the microcapsule drink does not induce changes in the cell cycle phase, yet it profoundly impacts all cells. Therefore, different concentrations of the probiotic miracle drink impede the cell cycle at distinct stages [48]. Lower drink concentrations inhibit the G2/M stage, while higher doses halt cells in the S stage. An exploration into the relationship between cell cycle arrest and gene activity in cancer cells reveals that MCF-7 cancer cells treated with the optimal ratio of probiotic nanoparticles exhibit simultaneous activation of the p34 protein kinase enzyme (cdc2) when arrested in the G2 phase [45]. Upon cell cycle arrest,

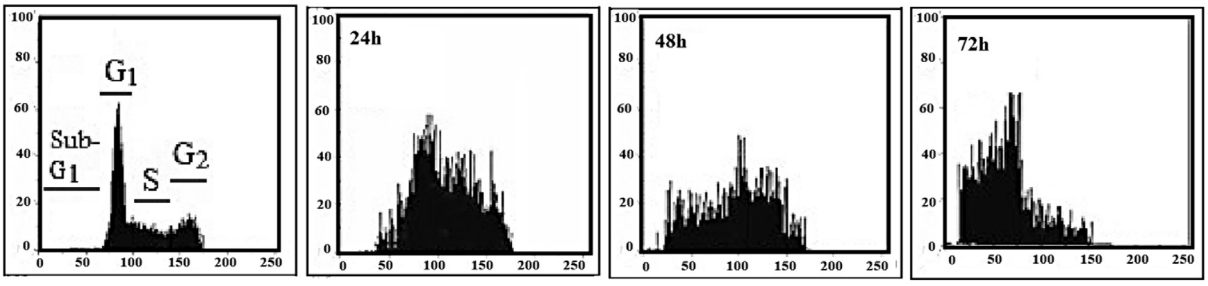

Fig. 9. Evaluation results of cell cycle evaluation of MCF7 cells treated with chitosan/alginate nanoparticles containing optimum *L. bulgaricus*.

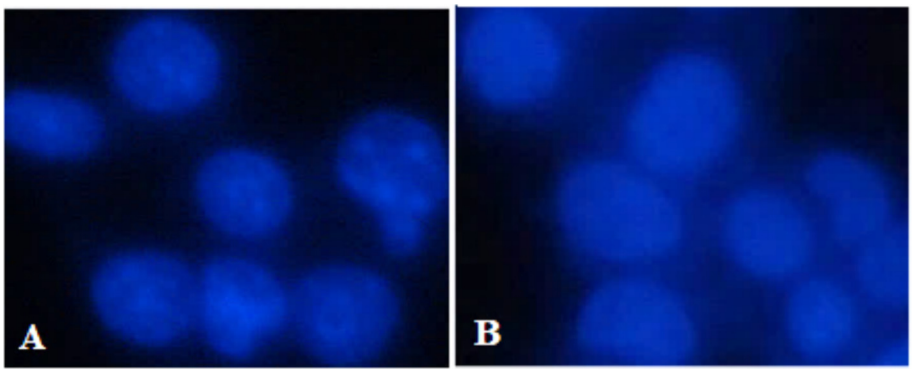

Fig. 10. Morphological changes induced in the absence (A) and presence (B) of optimal probiotic miraculous drink.

this enzyme undergoes re-phosphorylation, resulting in abnormal cell division and subsequent cell death. The extent of activation of these factors is dose-dependent, meaning alterations in drink dosage can influence the initiation or cessation of a series of genetic trends. Cell cycle arrest provides two potential outcomes for cells: repair or cell death [49]. Studies indicate the nucleotide excision repair system is not activated in MCF-7 cancer cells following probiotic treatment. This underscores the significance of the second factor, which involves DNA damage repair after cell cycle arrest. The results of this study indicate that increasing the dosage of the probiotic miracle drink leads to a higher number of cells being released into the medium, with the peak observed within the initial 48 h. This observation suggests a propensity for MCF-7 cancer cell lines to undergo apoptosis [50].

3.10. Evaluation of cell apoptosis using Hoechst staining

The outcomes of Hoechst staining 33,258 are depicted in Fig. 10. Normal cells exhibit uniform staining in this method, whereas apoptotic cell nuclei appear as pale blue dots due to chromatin condensation and nucleus fragmentation. Hoechst staining selectively binds to the adenine–thymine regions of the DNA molecule, resulting in the characteristic staining pattern. As previously mentioned, the negative control sample displays a uniform blue hue. However, when treated with the probiotic miracle drink, apoptotic cell nuclei adopt an irregular form and appear as vivid blue dots due to chromatin condensation and nucleus fragmentation.

4. Conclusions

This investigation focused on curbing the growth of MCF-7 breast cancer cells through a novel combination of miracle compounds utilizing *L. bulgaricus*-based probiotic microcapsules. A thorough comparison was made against the control treatment, following the formulation, preparation, and optimization of the ideal nanoparticle ratio. Also, it illustrates the cell cycle analysis of MCF-7 cancer cells compared to the control group, the G1 phase exhibited a larger cell volume of 120% compared to other phases. Ultimately, the study underscores the specific anti-cancer effects of the optimal treatment, which hinders the progression of cancer cells, as evidenced by the results of cellular tests.

CRediT authorship contribution statement

Kumars Jovaini: Data curation, Formal analysis, Funding acquisition, Investigation, Methodology, Project administration, Writing – original draft, Writing – review & editing. **Seyed Amir Mohammad Mortazavian Farsani:** Methodology, Supervision, Validation, Writing – review & editing. **Seyed Hamid Aghaee-Bakhtiari:** Conceptualization, Formal analysis, Visualization, Writing – original draft, Writing – review & editing. **Sahar Baniyaghoob:** Conceptualization, Data curation, Formal analysis, Investigation, Methodology, Project administration, Software, Writing – review & editing.

Conflict of interest

The authors declare that there are no conflicts of interest in this work.

Supplementary material

https://doi.org/10.1016/j.ejbt.2024.04.002.

Data availability

Data will be made available on request.

References

[1] McDonald ES, Clark AS, Tchou J, et al. Clinical diagnosis and management of breast cancer. J Nucl Med 2016;57(Suppl 1):9S–16S. https://doi.org/10.2967/jnumed.115.157834. PMid: 26834110.

[2] Steadman L, Rutter DR. Belief importance and the theory of planned behavior: Comparing modal and ranked modal beliefs in predicting attendance at breast screening. Br J Health Psychol 2004;9(4):447–63. https://doi.org/10.1348/1359107042304579. PMid: 15509354.

[3] Chen H, Shao F, Zhang F, et al. Association between dietary carrot intake and breast cancer. Medicine 2018;97(37):e12164. https://doi.org/10.1097/MD.0000000000012164. PMid: 30212943.

[4] Lamyian M, Hydarnia A, Ahmadi F, et al. Barriers to and factors facilitating breast cancer screening among Iranian women: A qualitative study. East Medit Health J 2007;13(5):1160–9. https://doi.org/10.26719/2007.13.5.1160. PMid: 18290410.

[5] Fisusi FA, Akala EO. Drug combinations in breast cancer therapy. Pharm Nanotechnol 2019;7(1):3–23. https://doi.org/10.2174/2211738507666190122111224. PMid: 30666921.

[6] Pondé N, Aftimos P, Piccart M. Antibody-drug conjugates in breast cancer: A comprehensive review. Curr Treat Options in Oncol 2019;20:37. https://doi.org/10.1007/s11864-019-0633-6. PMid: 30931493.

[7] Gilmour F, Williams A. Support with nutrition for women receiving chemotherapy for breast cancer. Br J Nurs 2018;27(4):S4–9. https://doi.org/10.12968/bjon.2018.27.4.S4. PMid: 29457937.

[8] Mishra A, Srivastava A, Pateriya A, et al. Metabolic reprogramming confers tamoxifen resistance in breast cancer. Chem Biol Interact 2021;347:. https://doi.org/10.1016/j.cbi.2021.109602. PMid: 34331906109602.

[9] Sachdev S, Carroll P, Sandler H, et al. Assessment of postprostatectomy radiotherapy as adjuvant or salvage therapy in patients with prostate cancer: A systematic review. JAMA Oncol 2020;6(11):1793–800. https://doi.org/10.1001/jamaoncol.2020.2832. PMid: 32852528.

[10] Jaganathan SK, Vellayappan MV, Narasimhan G, et al. Chemopreventive effect of apple and berry fruits against colon cancer. World J Gastroenterol 2014;20(45):17029–36. https://doi.org/10.3748/wjg.v20.i45.17029. PMid: 25493015.

[11] Przybylska K, Bennett RN, Kromer K, et al. Assessment of the antiproliferative activity of carrot and apple extract. Pol J Food Nutr Sci 2007;57(3):307–14.

[12] Mostafa HS, Ali MR, Mohamed RM. Production of a novel probiotic date juice with anti-proliferative activity against Hep-2 cancer cells. Food Sci Technol 2021;41(Supp 1):105–15. https://doi.org/10.1590/fst.09920.

[13] Le Leu RK, Hu Y, Brown IL, et al. Synbiotic intervention of *Bifidobacterium lactis* and resistant starch protects against colorectal cancer development in rats. Carcinogenesis 2009;31(2):246–51. https://doi.org/10.1093/carcin/bgp197. PMid: 19696163.

[14] Ohigashi S, Hoshino Y, Ohde S, et al. Functional outcome, quality of life, and efficacy of probiotics in postoperative patients with colorectal cancer. Surg Today 2011;41(9):1200–2127. https://doi.org/10.1007/s00595-010-4450-6.

[15] Taverniti V, Guglielmetti S. The immunomodulatory properties of probiotic microorganisms beyond their viability (ghost probiotics: Proposal of paraprobiotic concept). Genes Nutr 2011;6(3):261–9. https://doi.org/10.1007/s12263-011-0218-x.

[16] Gandomi H, Abbaszadeh S, Misaghi A, et al. Effect of chitosan-alginate encapsulation with inulin on survival of *Lactobacillus rhamnosus* GG during apple juice storage and under simulated gastrointestinal conditions. LWT Food Sci Technol 2016;69(11):365–71. https://doi.org/10.1016/j.lwt.2016.01.064.

[17] Hansen LT, Allan-Wojtas P, Jin YL, et al. Survival of Ca-alginate microencapsulated *Bifidobacterium* spp. in milk and simulated gastrointestinal conditions. Food Microbiol 2002;19(1):3–45. https://doi.org/10.1006/fmic.2001.0452.

[18] Petkova D, Mihaylova D, Desseva I. Microencapsulation in food industry – an overview. BIO Web Conf 2022;45:. https://doi.org/10.1051/bioconf/20224502005 02005.

[19] Abd El-Hack ME, El-Saadony MT, Shafi ME, et al. Antimicrobial and antioxidant properties of chitosan and its derivatives and their applications: A review. Int J Biol Macromol 2020;164:2726–44. https://doi.org/10.1016/j.ijbiomac.2020.08.153. PMid: 32841671.

[20] Yeung TW, Üçok EF, Tiani KA, et al. Microencapsulation in alginate and chitosan microgels to enhance viability of *Bifidobacterium longum* for oral delivery. Front Microbiol 2016;7:494. https://doi.org/10.3389/fmicb.2016.00494. PMid: 27148184.

[21] Mokriani S, Tukmechi A, Harzandi N, et al. *In vivo* murine breast cancer targeting by magnetic iron nanoparticles involving L. GG cytoplasmic fraction. Iran J Basic Med Sci 2021;24(5):682–9. https://doi.org/10.22038/ijbms.2021.54961.12322. PMid: 34249271.

[22] Zhang B, Guowei S, Bao C. Optimization of culture medium for *Lactobacillus bulgaricus* using Box-Behnken design. Acta Universitatis Cibiniensis Series E: Food Technol 2017;21(1):3–10. https://doi.org/10.1515/aucft-2017-0001.

[23] Deding U, Baatrup G, Kaalby L, et al. Carrot intake and risk of developing cancer: A prospective cohort study. Nutrients 2023;15(3):678. https://doi.org/10.3390/nu15030678. PMid: 36771385.

[24] Lechner JF, Stoner GD. Red beetroot and betalains as cancer chemopreventative agents. Molecules 2019;24(8):1602. https://doi.org/10.3390/molecules24081602. PMid: 31018549.

[25] Zohri M, Arefian E, Javar HA, et al. Potential of chitosan/alginate nanoparticles as a non-viral vector for gene delivery: Formulation and optimization using D-optimal design. Mater Sci Eng C 2021;128:. https://doi.org/10.1016/j.msec.2021.112262. PMid: 34474821112262.

[26] Karimi Zindashti G, Khaleghi S, Nemati Mansur F, et al. The design and preparation of fluorescent labeled chitosan nanoparticles for intestinal delivery. Med Sci J Islamic Azad Univ 2020;30(4):352–62. https://doi.org/10.29252/iau.30.4.352.

[27] Riaz Rajoka MS, Zhao H, Lu Y, et al. Anticancer potential against cervix cancer (HeLa) cell line of probiotic *Lactobacillus casei* and *Lactobacillus paracasei* strains isolated from human breast milk. Food Funct 2018;9(5):2705–15. https://doi.org/10.1039/C8FO00547H. PMid: 29762617.

[28] Budi S, Suliasih BA, Erdawati IR. Size-controlled chitosan nanoparticles prepared using ionotropic gelation. ScienceAsia 2020;46:457–61. https://doi.org/10.2306/scienceasia1513-1874.2020.059.

[29] Sarei F, Mohammadpour Dounighi N, Zolfagharian H, et al. Design and evaluate alginate nanoparticles as a protein delivery system. Arch Razi Inst 2013;68(2):139–46.

[30] Oberoi K, Tolun A, Altintas Z, et al. Effect of alginate-microencapsulated hydrogels on the survival of *Lactobacillus rhamnosus* under simulated gastrointestinal conditions. Foods 2021;10(9):1999. https://doi.org/10.3390/foods10091999. PMid: 34574109.

[31] Lee KY, Heo TR. Survival of *Bifidobacterium longum* immobilized in calcium alginate beads in simulated gastric juices and bile salt solution. Appl Environ Microbiol 2000;66(2):869–73. https://doi.org/10.1128/AEM.66.2.869-873.2000. PMid: 10653768.

[32] Zohri M, Akbari Javar H, Gazori T, et al. Response Surface Methodology for statistical optimization of chitosan/alginate nanoparticles as a vehicle for recombinant human bone morphogenetic protein-2 delivery. Int J Nanomed 2020;15:8345–56. https://doi.org/10.2147/IJN.S250630. PMid: 33154637.

[33] Nematollahi A, Sohrabvandi S, Mortazavian AM, et al. Viability of probiotic bacteria and some chemical and sensory characteristics in cornelian cherry juice during cold storage. Electron J Biotechnol 2016;21:49–53. https://doi.org/10.1016/j.ejbt.2016.03.001.

[34] Zohri M, Nomani AR, Gazori T, et al. Characterization of chitosan/alginate self assembled nanoparticles as a protein carrier. J Dispers Sci Technol 2011;32(4):576–82. https://doi.org/10.1080/01932691003757314.

[35] Alkushi AG, Abdelfattah-Hassan A, Eldoumani H, et al. Probiotics-loaded nanoparticles attenuated colon inflammation, oxidative stress, and apoptosis in colitis. Sci Rep 2022;12:5116. https://doi.org/10.1038/s41598-022-08915-5. PMid: 35332200.

[36] Shanmugam R, Munusamy T, Jayakodi S, et al. Probiotic-bacteria (*Lactobacillus fermentum*)-wrapped zinc oxide nanoparticles: Biosynthesis, characterization, and antibacterial activity. Fermentation 2023;9(5):413. https://doi.org/10.3390/fermentation9050413.

[37] Dimitrellou D, Kandylis P, Lević S, et al. Encapsulation of *Lactobacillus casei* ATCC 393 in alginate capsules for probiotic fermented milk production. LWT 2023;116:. https://doi.org/10.1016/j.lwt.2019.108501108501.

[38] Shah A, Lutfullah G, Ahmad K, et al. *Daphne mucronata*-mediated phytosynthesis of silver nanoparticles and their novel biological applications, compatibility and toxicity studies. Green Chem Lett Rev 2018;11(3):318–33. https://doi.org/10.1080/17518253.2018.1502365.

[39] Koo SM, Cho YH, Huh CS, et al. Improvement of the stability of *Lactobacillus casei* YIT 9018 by microencapsulation using alginate and chitosan. J Microbiol Biotechnol 2001;11(3):376–83.

[40] Tantra R, Schulze Ph, Quincey P. Effect of nanoparticle concentration on zeta-potential measurement results and reproducibility. Particuology 2010;8(3):279–85. https://doi.org/10.1016/j.partic.2010.01.003.

[41] Azuma K, Osaki T, Minami S, et al. Anticancer and anti-inflammatory properties of chitin and chitosan oligosaccharides. J Funct Biomater 2019;6(1):33–49. https://doi.org/10.3390/jfb6010033. PMid: 25594943.

[42] Chen ZY, Hsieh YM, Huang CC, et al. Inhibitory effects of probiotic *Lactobacillus* on the growth of human colonic carcinoma cell line HT-29. Molecules 2017;22(1):107. https://doi.org/10.3390/molecules22010107. PMid: 28075415.

[43] Shakil MS, Mahmud KM, Sayem M, et al. Using chitosan or chitosan derivatives in cancer therapy. Polysaccharides 2021;2(4):795–816. https://doi.org/10.3390/polysaccharides2040048.

[44] Er S, Koparal AT, Kivanç M. Cytotoxic effects of various lactic acid bacteria on Caco-2 cells. Turk. J. Bio 2015;39(1):4. https://doi.org/10.3906/biy-1402-62.

[45] Niu T, Zhang W, Xiao W. MicroRNA regulation of cancer stem cells in the pathogenesis of breast cancer. Cancer Cell Int 2021;21(1):31. https://doi.org/10.1186/s12935-020-01716-8. PMid: 33413418.

[46] Päth G, Bornstein SR, Gurniak M, et al. Human breast adipocytes express interleukin-6 (IL-6) and its receptor system: Increased IL-6 production by β-adrenergic activation and effects of IL-6 on adipocyte function. J Clin Endocrinol Metab 2001;86(5):2281–8. https://doi.org/10.1210/jcem.86.5.7494. PMid: 11344240.

[47] Wang L, Jin Z, Master RP, et al. Breast cancer stem cells: Signaling pathways, cellular interactions, and therapeutic implications. Cancers 2022;14(13):3287. https://doi.org/10.3390/cancers14133287. PMid: 35805056.
[48] Yousefnia S, Seyed Forootan F, Seyed Forootan S, et al. Mechanistic pathways of malignancy in breast cancer stem cells. Front Oncol 2020;10:452. https://doi.org/10.3389/fonc.2020.00452. PMid: 32426267.
[49] Gupta M, Walters BA, Katsara O, et al. eIF2Bδ blocks the integrated stress response and maintains eIF2B activity and cancer metastasis by overexpression in breast cancer stem cells. Proc Natl Acad Sci USA 2023;120(15):. https://doi.org/10.1073/pnas.2207898120. PMid: 37014850e2207898120.
[50] Fan B, Shi S, Shen X, et al. Effect of HMGN2 on proliferation and apoptosis of MCF-7 breast cancer cells. Oncol Lett 2019;17(1):1160–6. https://doi.org/10.3892/ol.2018.9668.